JOURNAL OF SPACECRAFT AND ROCKETS
Vol. 46, No. 3, May–June 2009

Effective Thermal/Mechanical Properties of Honeycomb Core Panels for Hot Structure Applications

J. Fatemi*
Dutch Space, 2303 DB Leiden, The Netherlands
and
M. H. J. Lemmen†
Netherlands Organization for Applied Scientific Research, 2600 AD Delft, The Netherlands

DOI: 10.2514/1.30408

The present work addresses the computation of the effective thermal and mechanical properties of a honeycomb-core sandwich panel. The panel considered has a hexagon-cell honeycomb core. An alternative method, based on the Gebhart factors within a hexagonal cell, is presented in addition to the familiar Swann–Pittman method. The advantage of the alternative method is that it incorporates different emissivities for both face sheets and honeycomb and that it can easily be extended through this method with in-plane effective conductivity values for the honeycomb core. The effective mechanical properties of the core are determined using the mechanics of materials method. The effective continuum properties are then used with classical laminate theory to construct an equivalent laminate structure to replace the honeycomb-core sandwich panel. The thermal and thermomechanical behavior of the equivalent laminate structure is compared with that of the detailed model of the honeycomb-core sandwich panel using finite element analysis. The results of the study show that the proposed equivalent laminate structure accurately captures the thermal and thermomechanical behavior of the original honeycomb-core sandwich panel with very low computational costs.

Nomenclature

A	=	area, m^2
B	=	radiative exchange (Gebhart) factor
C	=	conduction, W/K
C_p	=	thermal heat capacity, J/kg K
d	=	height (of core) (Fig. 1), m
E	=	modulus of elasticity, N/m^2
F	=	view factor
G	=	shear modulus of elasticity, N/m^2
k	=	thermal conductivity, W/m K
L	=	conductive length (of unit cell), m
q	=	heat flow, W
r	=	radius, m
S	=	size of honeycomb cell (Fig. 1), m
T	=	temperature, K
t	=	thickness, m
α	=	coefficient of thermal expansion, m/m K
ΔA	=	cross-sectional area of the conductive path though the core material, m^2
ε	=	emissivity
ρ	=	material density, kg/m^3
σ	=	Stefan–Boltzmann radiation constant, 5.670×10^{-08}, $W\,m^{-2}\,K^{-4}$

Subscripts:

avg	=	average (of honeycomb/sandwich)
c	=	core (honeycomb cell)
cm	=	core material (for Swann–Pittman emissivity, average value of both face sheets is used)
direct	=	radiative exchange between face sheets (including multiple reflections)
eff	=	effective
eq	=	equivalent area
f	=	face sheet
gas	=	gas (within the honeycomb core)
hex	=	hexagonal wall
i, j	=	integer index for nonspecific surface number
indirect	=	radiative exchange between honeycomb core and face sheets (including multiple reflections)
L	=	length direction of the honeycomb (Fig. 1)
rad	=	radiative
T	=	thickness direction of the honeycomb (Fig. 1)
total	=	total combined effect of all contributions
W	=	width direction of the honeycomb (Fig. 1)
1	=	hot top face sheet
2	=	colder bottom face sheet

Presented as Paper 8121 at the 14th AIAA/AHI Space Planes and Hypersonic Systems and Technologies Conference, Canberra, Australia, 6–9 November 2006; received 12 February 2007; revision received 29 December 2008; accepted for publication 29 December 2008.

*Senior Mechanical Engineer, Post Office Box 32070; j.fatemi@dutchspace.nl. Member AIAA.

†Thermal/Mechanical Engineer, Science and Industry Division, Post Office Box 155; martin.lemmen@tno.nl.

I. Introduction

THE aerodynamic surface design of the current generation of reusable launch vehicle (RLV) is typically based on a load-carrying cold structure surrounded by a thermal protection system (TPS). The main function of the TPS is to maintain the vehicle structural temperature within acceptable limits and also to provide an acceptable aerodynamic surface to prevent premature transition to turbulent flow during the atmospheric reentry. To improve the reusability and to reduce the mass of the RLVs with the objective of access to space cost reduction, load-carrying metallic TPS are under development. This type of structure can be used as a hot structure (e.g., control surface) or as a load-carrying skin component of a TPS, in combination with an inner insulating layer. This load-carrying structure component may consist of an assembly of honeycomb-core panels, made of high-temperature metal alloys, which is able to resist the thermal and aerodynamic loads during the atmospheric reentry.

Finite element (FE) methods are used to predict the mechanical and thermomechanical responses of the TPS to the external aerodynamic loads (aerodynamic heating and forces). The accuracy of response quantities predicted by FE models of sandwich structures

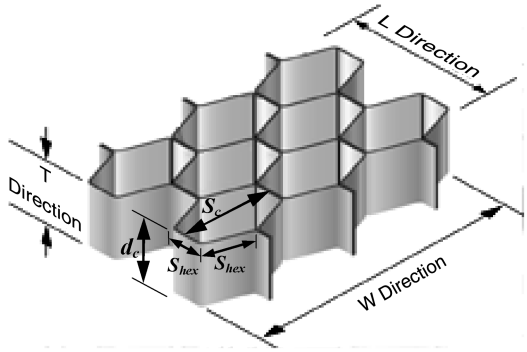

Fig. 1 Honeycomb characteristics.

depends on a large number of material and geometric parameters of the face sheets and the core. The computational effort associated with detailed FE models of honeycomb-core sandwich panels increases very rapidly with the increase in the number of cells in the panel core, especially when a large aerodynamic surface of the vehicle should be modeled. For this reason, the analysis of large-scale sandwich panel structures can be done with detailed FE models, but computational resources required are limiting.

The sandwich panel considered in this study is composed of two metallic face sheets perfectly bonded to a metallic honeycomb core (made from hexagonal cells) by means of a brazing process. Face sheets and honeycomb core are made of oxide dispersion strengthened (ODS) alloys PM1000 and PM2000, respectively. Such a sandwich panel concept has already been developed for application to a hot metal control surface for RLVs [1]. The different materials of face sheets and honeycomb-core material, with very different surface emissivities and the relative large thickness of the core material, increased the need for an alternative method for modeling the heat transfer through the sandwich structure, which would be able to incorporate different optical properties of the materials and also be able to take into account the effective in-plane conductivity of the honeycomb structure.

To model the heat transfer through the thickness of such honeycomb-core panels, an alternative analytical method based on an approximation for radiative heat exchange within one honeycomb cell is presented in this paper in addition to the familiar semi-analytical Swann–Pittman relation [2]. The two methods transform the radiative heat transfer in the honeycomb into an effective temperature-dependent conductive relation. The advantage of the alternative method is that it considers a function of the emissivity of both face sheets and honeycomb. The method forms a basis by which the in-plane effective conductivity values for the honeycomb core can also be analyzed. The alternative method offers advantages over the Swann–Pittman method for thick honeycomb cores, situations where the core and face emissivities differ significantly, and areas of the vehicle where in-plane conduction is important (areas of the vehicle where the spatial heat flux gradients are large, e.g., near the leading edges).

Having calculated the equivalent conductive properties for radiation and convection, the honeycomb core can then be replaced by an equivalent shell layer in the sandwich panel. The calculated thermal properties for the equivalent shell layer are orthotropic and temperature-dependent. In the subsequent FE analysis, the combination of two skins and one equivalent shell in the sandwich panel will be represented as a laminated shell structure. This type of modeling will decrease, to a large extent, the size and complexity of the FE model and thus reduce computational time/cost, while maintaining an acceptable level of accuracy. Hence, this method is very beneficial for support of design trade studies in the conceptual design phase for RLVs [3].

The effective mechanical properties of honeycomb-core sandwich panel are calculated in two steps. The first step consists of predicting the effective properties of the honeycomb core in terms of its geometric and material characteristics by means of mechanics of materials approach. The effective elastic properties determined in the first step are used in conjunction with the classical laminate theory to determine the overall structural behavior of the entire sandwich structure. It should be highlighted that such method has already been implemented in some commercial packages (e.g., see [3]).

The proposed approaches are used to estimate the effective thermal and mechanical properties of a honeycomb-core sandwich panel. The thermal and thermomechanical behavior of the equivalent models is compared with the behavior of the detailed FE model of the sandwich panel.

II. Equivalent Continuum Thermal Properties of Honeycomb Core

The following section outlines the methods for the estimation of equivalent thermal properties of honeycomb core. The parameters used in the analyses are graphically presented in Fig. 1.

The heat flow through the core for both methods can be defined as

$$q_{\text{total}} = k_{c,\text{eff}} \frac{A}{d_c}(T_1 - T_2) = \left[k_{\text{cm}} \frac{\Delta A}{A} + k_{c,\text{gas}} \left(1 - \frac{\Delta A}{A}\right) + k_{c,\text{rad}} \right] \frac{A}{d_c}(T_1 - T_2) \tag{1}$$

The factor ΔA (cross-sectional area of the core) for the hexagonal cell can be expressed as $\Delta A = 4 \cdot S_{\text{hex}} \cdot t_c$ (with $S_{\text{hex}} = \frac{1}{3}\sqrt{3} S_c$) for a representative cell area, assuming the location of the honeycomb joints consists of a double wall, or $\Delta A = 3 \cdot S_{\text{hex}} \cdot t_c$ assuming the joints consist of a single wall, as is assumed in this paper. The representative area (in T direction) of one honeycomb cell can be expressed by $A = 1.5 \times S_{\text{hex}} \times S_c = \frac{1}{2}\sqrt{3} S_c^2$.

The equivalent gas conductance coefficient $k_{c,\text{gas}}$ can be calculated using the relations from Blosser [4]. However, for our RLV example, a vacuum condition is assumed for the presented case study in this paper. As a consequence, $k_{c,\text{gas}}$ is nullified (the order of magnitude of $k_{c,\text{gas}}$ is 10^{-5} at a pressure of 10^{-3} Pa).

A. Swann–Pittman Model for Effective Conductivity in Thickness Direction

The effective thermal conductivity of the honeycomb core is calculated using the Swann–Pittman [2] semi-analytical model. Solid conduction through the honeycomb cell walls, gas conduction in the honeycomb cells (nullified in the case study because of vacuum condition), and heat transfer by radiation in the honeycomb cell enclosure are considered heat transfer mechanisms in this approach. The effective thermal conductivity depends on the core geometry and material properties, the properties of the gas in the cell, and the temperatures of the two face sheets.

The Swann–Pittman effective thermal conductivity relation is defined as follows:

$$k_{c,\text{eff}} = k_{\text{cm}} \frac{\Delta A}{A} + k_{c,\text{gas}} \left(1 - \frac{\Delta A}{A}\right) + k_{c,\text{rad}} \tag{2}$$

where $k_{c,\text{rad}}$ is the effective conductivity caused by radiative heat transfer:

$$k_{c,\text{rad}} = 0.664 \left(\frac{d_c}{S_c} + 0.3\right)^{-0.69} \varepsilon_{\text{cm}}^{1.63\left(\frac{d_c}{S_c}+1\right)^{-0.89}} d_c \sigma (T_1 + T_2)(T_1^2 + T_2^2) \tag{3}$$

To model the radiative heat transfer through the honeycomb as a material property, the radiative heat transfer coefficient has to be temperature dependent. Two new terms, $T_{\text{avg}} = \frac{1}{2}(T_1 + T_2)$ being average honeycomb temperature and $\Delta T = T_1 - T_2$ being temperature gradient, are defined. Applying these definitions in Eq. (3) results in

$$k_{c,\mathrm{rad}} = 0.664\left(\frac{d_c}{S_c}+0.3\right)^{-0.69}\varepsilon_{\mathrm{cm}}^{1.63(\frac{d_c}{S_c}+1)^{-0.89}} d_c\sigma \times 2T_{\mathrm{avg}} \times \left[\left(T_{\mathrm{avg}}+\frac{1}{2}\Delta T\right)^2+\left(T_{\mathrm{avg}}-\frac{1}{2}\Delta T\right)^2\right] = 0.664\left(\frac{d_c}{S_c}+0.3\right)^{-0.69}\varepsilon_{\mathrm{cm}}^{1.63(\frac{d_c}{S_c}+1)^{-0.89}} d_c\sigma \times 4T_{\mathrm{avg}}^3\left[1+\left(\frac{\Delta T}{2T_{\mathrm{avg}}}\right)^2\right] \quad (4)$$

Neglecting the quadratic term in Eq. (4) results in an error in the effective conductivity calculation. However, the error is small when the difference between the cold and hot temperatures is limited (as an example, for a hot face temperature of 1100 K and a cold face temperature of 900 K, the relative error is 1%, which lies within the accuracy of the relation itself). For structures with a significantly larger relative gradient, one should be aware of decreased accuracy of the results of this method. The effective conductivity, caused by radiative heat transfer, can now be expressed as

$$k_{c,\mathrm{rad}} = 2.656\left(\frac{d_c}{S_c}+0.3\right)^{-0.69}\varepsilon_{\mathrm{cm}}^{1.63(\frac{d_c}{S_c}+1)^{-0.89}} d_c\sigma T_{\mathrm{avg}}^3 \quad (5)$$

For the radiative heat transfer through the core to be treated as a temperature-dependent effective thermal conductivity, it is assumed that T_{avg} is the temperature of the core material and does not depend directly on the face sheet temperatures. The total heat flow trough the thickness of the sandwich panel can now be calculated using Eq. (1).

B. Alternative Method for Analysis of Effective Conductivity

An alternative method for the effective conductance through the honeycomb core of a sandwich panel is presented in this section. The need for such a method has risen in the case study presented in this paper, consisting of a sandwich panel with a core made of PM2000 and face sheets made of PM1000 with different emissivities. This resulted in the need for an alternative relation containing the emissivities of both PM1000 and PM2000. Also, the core thickness of the case study is relatively large, and so the in-plane conductance of the honeycomb core becomes an issue. Swann–Pittman [2] does not provide the in-plane effective conductivity of the honeycomb core.

Because the ODS sandwich panel is designed to be used for reentry vehicles, the in-plane thermal gradient can play a significant role in the thermal stress of the load-carrying skin. Therefore, it is important to model the in-plane conductance as accurately as possible.

This alternative method is based on the radiative exchange factors of Gebhart [5] for a hexagonal cell shape. To calculate these radiative exchange factors, the view factors within a hexagonal cell are first calculated. For the effective conduction through the thickness of the honeycomb core, a simple three-surface model (Fig. 2) is used to calculate the geometrical view factors (sometimes referred as configuration factors), which is the fraction of the radiant energy emitted by surface i which is directly intercepted by surface j.

For the case study presented in this paper, the honeycomb geometry characteristics (see Fig. 1) are as follows:

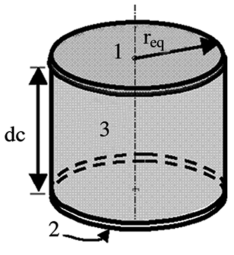

Fig. 2 Equivalent cylinder surfaces.

Table 1 Hexagon + equivalent cylinder areas

	A_{hex},m^2	A_{eq},m^2
1, top	5.543E-05	5.543E-05
2, bottom	5.543E-05	5.543E-05
3, side	2.702E-04	2.639E-04

Honeycomb cell size is $S_c = 0.008$ m.
Honeycomb-core height is $d_c = 0.01$ m.
Honeycomb-core cell wall thickness is $t_c = 0.125 \times 10^{-3}$ m.
Face sheets thickness is $t_f = 0.25 \times 10^{-3}$ m.To keep the view-factor relation simple and analytical, the hexagonal cell is approximated by a cylinder with the same cross-sectional area. For this, an equivalent radius is needed:

$$A_{\mathrm{hex}} = \pi r_{\mathrm{eq}}^2 = \tfrac{1}{2}\sqrt{3}S_c^2$$

which results in $r_{\mathrm{eq}} = \sqrt{\frac{1}{2\pi}\sqrt{3}} \times S_c = 0.0042$ m. This results in the areas shown in Table 1 for the selected case study.

Using the relation from Sparrow and Cess [6], the view factor F_{12} between two disks with radius r_{eq} separated by a distance d_c can be written as

$$F_{12} = \tfrac{1}{2}(Z - \sqrt{Z^2-4}) \quad (6)$$

with $Y = d_c/r_{\mathrm{eq}}$, $Z = 2 + Y^2$. This results in a view factor $F_{12} = 0.1327$ for our case study.

The other view factors can be deduced by the enclosure relation and the reciprocity relation. The enclosure relation states that for surfaces within an enclosure

$$\sum_j F_{ij} = 1 \quad (7)$$

The reciprocity relation states

$$A_i F_{ij} = A_j F_{ji} \Rightarrow F_{21} = \frac{A_1}{A_2}F_{12} \quad (8)$$

This results in the view factor matrix presented in Table 2.

Comparing these results with those of a hexagon determined by Feingold [7] (linearly interpolated) for an L factor (hexagonal side S_{hex}/core height) of 0.46188, results in $F_{12} = 0.13265$. The approximation of the hexagonal cell with a cylinder proves to be very accurate (relative error <0.1%). The numerical results of the case study are shown as an example. The relations are kept analytical and parametric so that the results are easily adjusted for different properties. This way they can also contain temperature-dependent properties (e.g., emissivity).

To determine the radiative exchange between the different honeycomb surfaces, the view factors have to be transformed into radiative exchange factors, using the Gebhart [5] method. For diffuse opaque surfaces, these radiative exchange factors (here called Gebhart factors) can be calculated, defined as the ratio between energy absorbed by surface j and the energy emitted by surface i, including the reflections of all other interacting surfaces, according to

$$B_{ij} = F_{ij}\varepsilon_j + \sum_k (1-\varepsilon_k)F_{ik}B_{kj} \quad (9)$$

For gray surfaces (with temperatures of the same order of magnitude) the following reciprocity is also valid:

$$\varepsilon_i A_i B_{ij} = \varepsilon_j A_j B_{ji} \quad (10)$$

With these relations, the Gebhart factors can iteratively be calculated, assuming for the case study an emissivity factor of 0.80 for the PM1000 face sheets and 0.55 for the PM2000 honeycomb. These emissivity values can consequently be made temperature dependent, to represent the actual (tested) emissivity of both materials. The resulting Gebhart factors are shown in Table 3.

Table 2 View factor of three-surface cylinder

$i\backslash j$	1	2	3
1	0	$F_{12} = 0.1327$	$F_{13} = 1\text{-}F_{12} = 0.8673$
2	$F_{21} = F_{12} = 0.1327$	0	$F_{23} = 1\text{-}F_{21} = 0.8673$
3	$F_{31} = (A_1/A_3) \cdot F_{13} = 0.1821$	$F_{32} = F_{31} = 0.1821$	$F_{33} = 1\text{-}F_{31}\text{-}F_{32} = 0.6357$

Table 3 Gebhart factors of three-surface cylinder ($\varepsilon_f = 0.80$, $\varepsilon_c = 0.55$)

$i\backslash j$	1	2	3
1	0.09047	0.19389	0.71565
2	0.19389	0.09047	0.71565
3	0.21861	0.21861	0.56277

The radiative heat flow from the hot to cold face sheet can now be expressed as

$$q_{ij} = \varepsilon_i A_i B_{ij} \sigma (T_i^4 - T_j^4) \tag{11}$$

The total radiative heat flow exchange relation [comparable to Eq. (1)] can now be written by

$$\begin{aligned} q_{12,\mathrm{rad}} &= k_{c,\mathrm{rad}} \frac{A}{d_c}(T_1 - T_2) \\ &= (k_{c,\mathrm{rad,direct}} + k_{c,\mathrm{rad,indirect}}) \frac{A}{d_c}(T_1 - T_2) \end{aligned} \tag{12}$$

In Eq. (12), the direct part is defined as the radiative exchange between the face sheets. The indirect part is represented by radiative exchange between the honeycomb core and the face sheets, which cannot be neglected. These thermal paths are illustrated in Fig. 3.

The effective conductivity caused by the radiation between face sheets can be written as

$$\begin{aligned} k_{c,\mathrm{rad,direct}} &= \varepsilon_1 B_{12} d_c \sigma (T_1 + T_2)(T_1^2 + T_2^2) \\ &= \varepsilon_1 B_{12} d_c \sigma \cdot 4T_{\mathrm{avg}}^3 \left[1 + \left(\frac{\Delta T}{2T_{\mathrm{avg}}} \right)^2 \right] \end{aligned} \tag{13}$$

Again neglecting the quadratic term in this formula (relative error in $k_{c,\mathrm{rad,direct}}$ is less than 1%, for a temperature gradient less than 20% of T_{avg}), the direct radiative heat exchange can be approximated by

$$k_{c,\mathrm{rad,direct}} = \varepsilon_1 B_{12} d_c \sigma \cdot 4T_{\mathrm{avg}}^3 \tag{14}$$

Taking only the direct radiation from hot to cold face sheet into account would ignore the amount of heat that is radiated from the hot face sheet that is absorbed by the honeycomb (and conductively transferred to the cold face sheet). Similarly, the heat radiated from the honeycomb that is absorbed by the cold face sheet would also be ignored.

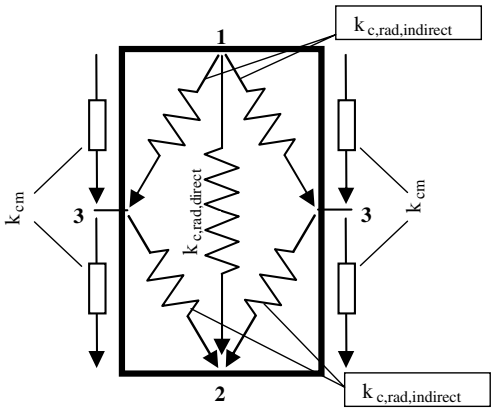

Fig. 3 Thermal path diagram.

If the honeycomb radiative average temperature is assumed to be T_{avg}, the indirect part of the radiation can be assigned to an indirect effective conductivity (ignoring again the quadratic terms) by

$$\left.\begin{aligned} k_{c,\mathrm{rad},13} &= \varepsilon_1 \frac{A_1}{A_1} B_{13} \cdot \frac{1}{2} d_c \sigma \cdot 4T_{\frac{1}{4}}^3 = \varepsilon_1 B_{13} \cdot \frac{1}{2} d_c \sigma \cdot 4T_{\frac{1}{4}}^3 \\ k_{c,\mathrm{rad},32} &= \varepsilon_3 \tfrac{A_3}{A_1} B_{32} \cdot \tfrac{1}{2} d_c \sigma \cdot 4T_{\frac{3}{4}}^3 \\ \varepsilon_3 A_3 B_{32} &= \varepsilon_2 A_2 B_{23} = \varepsilon_1 A_1 B_{13} \end{aligned}\right\} k_{c,\mathrm{rad},32} = \varepsilon_1 B_{13} \cdot \frac{1}{2} d_c \sigma \cdot 4T_{\frac{3}{4}}^3 \tag{15}$$

with $T_{\frac{1}{4}}$ being the average of the hot face sheet temperature T_1 and T_{avg}, and $T_{\frac{3}{4}}$ being the average of the cold face sheet temperature T_2 and T_{avg}. These conductivities are assumed to be coupled in series, so that

$$k_{c,\mathrm{rad,indirect}} = k_{c,\mathrm{rad},13+32} = \frac{2 \cdot k_{c,\mathrm{rad},13} \cdot k_{c,\mathrm{rad},32}}{k_{c,\mathrm{rad},13} + k_{c,\mathrm{rad},32}} \tag{16}$$

This results in an indirect effective conductivity of

$$k_{c,\mathrm{rad,indirect}} = 4\varepsilon_1 B_{13} d_c \sigma \frac{T_{\frac{1}{4}}^3 T_{\frac{3}{4}}^3}{T_{\frac{1}{4}}^3 + T_{\frac{3}{4}}^3} \tag{17}$$

Since $T_{\frac{1}{4}} = T_{\mathrm{avg}} + \frac{1}{4}\Delta T$ and $T_{\frac{3}{4}} = T_{\mathrm{avg}} - \frac{1}{4}\Delta T$, the last part of Eq. (17) can be simplified as follows:

$$\begin{aligned} \frac{T_{1/4}^3 T_{3/4}^3}{T_{1/4}^3 + T_{3/4}^3} &= \frac{[T_{\mathrm{avg}} + (1/4)\Delta T]^3 [T_{\mathrm{avg}} - (1/4)\Delta T]^3}{[T_{\mathrm{avg}} + (1/4)\Delta T]^3 + [T_{\mathrm{avg}} - (1/4)\Delta T]^3} \\ &= \frac{[T_{\mathrm{avg}}^2 - (1/16)\Delta T^2]^3}{2T_{\mathrm{avg}}^3 + (3/16)T_{\mathrm{avg}}\Delta T^2} \approx \frac{T_{\mathrm{avg}}^6 + \mathcal{O}(T_{\mathrm{avg}})^4}{2T_{\mathrm{avg}}^3 + \mathcal{O}(T_{\mathrm{avg}})} \approx \frac{1}{2} T_{\mathrm{avg}}^3 \end{aligned} \tag{18}$$

which leads to

$$k_{c,\mathrm{rad,indirect}} \approx \tfrac{1}{2}\varepsilon_1 B_{13} d_c \sigma \cdot 4T_{\mathrm{avg}}^3 \tag{19}$$

Neglecting the lower order terms (for a hot face temperature of 1100 K and a cold face temperature of 900 K, the relative error in $k_{c,\mathrm{rad,indirect}}$ is less than 2%) makes it possible to define this conductivity as a property solely dependent on the core temperature. However, the inaccuracy associated with the assumption that the temperature gradient through the sandwich is linear is more difficult to estimate, as well as the inaccuracy in the use of the average honeycomb temperature in combination with the Gebhart factor of the entire honeycomb wall (as if uniform in temperature). Because the temperature profile in the equivalent laminate is not linear, the error is assessed by comparing the temperature profiles of the equivalent structures with the detailed FE analysis results. This assessment is presented in Sec. V.

Adding the direct and indirect parts of the radiative exchange within the honeycomb core results in the following final relation for the effective conductivity in thickness direction of a honeycomb-core sandwich panel as computed by the alternative method

$$\begin{aligned} k_{c.\mathrm{eff}} &= k_{\mathrm{cm}} \frac{\Delta A}{A} + k_{c,\mathrm{rad}} = k_{\mathrm{cm}} \frac{\Delta A}{A} + (k_{c,\mathrm{rad,direct}} + k_{c,\mathrm{rad,indirect}}) \\ &= k_{\mathrm{cm}} \frac{\Delta A}{A} + \left(\varepsilon_1 B_{12} + \frac{1}{2}\varepsilon_1 B_{13} \right) d_c 4\sigma T_{\mathrm{avg}}^3 \end{aligned} \tag{20}$$

C. In-Plane Effective Conductivity Through the Honeycomb Core

For the in-plane effective conductivity through the honeycomb core, similar factors can be derived based on the radiative exchange factors between the honeycomb cell walls.

1. Conduction in the L Direction

The conduction in the L direction (see Fig. 1) can be found by simple conductive relations. The conduction for one equivalent cell area is $C_L = 2k_{\text{cm}}t_c d_c/2 \cdot S_{\text{hex}}$. The effective length of a cell area in the L direction is $L_L = 1.5 \times S_{\text{hex}}$ and the cross-sectional effective area of one cell in the L direction is $A_L = S_c d_c$.

The effective conductivity of one cell in the L direction can be written as follows:

$$k_{c,\text{eff},L} = \frac{C_L L_L}{A_L} \tag{21}$$

Replacing C_L, L_L, and A_L in Eq. (21) results in the following expression for the effective conductivity:

$$k_{c,\text{eff},L} = \frac{1.5k_{\text{cm}}t_c}{S_c} \tag{22}$$

2. Conduction in the W Direction

The effective conductivity of one cell in the W direction can be written as follows:

$$k_{c,\text{eff},W} = \frac{C_W L_W}{A_W} \tag{23}$$

Assuming a perfect thermal contact in the honeycomb joints, the effective conduction in the W direction for one equivalent cell area can be expressed by the following relation:

$$C_W = \frac{k_{\text{cm}}t_c d_c}{2 \cdot S_{\text{hex}}} \tag{24}$$

The effective length of a cell area in the W direction is $L_W = S_c$, and the cross-sectional effective area of one cell in the W direction is $A_W = 1.5ACd_c$. Using these definitions, the effective conductivity of one cell in the W direction can be expressed by

$$k_{c,\text{eff},W} = \frac{1}{3} \cdot \frac{k_{\text{cm}}t_c S_c}{S_{\text{hex}}^2} \tag{25}$$

The effective conduction part caused by radiation for both in-plane directions is analyzed in the next section.

3. Radiation in the L and W Directions

To analyze the radiative exchange within a honeycomb cell, the cell wall is divided into two halves, denoted by 3 and 4 in Fig. 4. The hexagonal cell is simplified into the cylindrical shape with the cylinder part divided into two halves.

To determine the radiative exchange factor (Gebhart factor) from one cell wall (A_3) to the opposite (A_4), the view factor F_{34} needs to be calculated. F_{12} is known by Eq. (6), which is 0.1327 in our case study. Knowing F_{12}, other view factors can be calculated as follows: $F_{13} = F_{14} = F_{23} = F_{24} = \frac{1}{2}(1 - F_{12}) = 0.4336$. Using the reciprocity relation (10), $F_{31}(=F_{41} = F_{32} = F_{42})$ can be calculated:

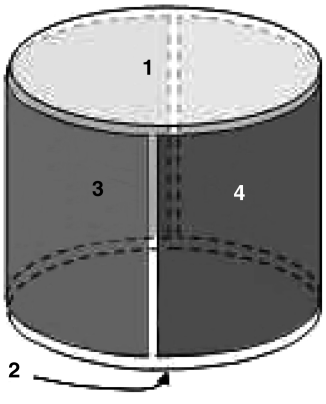

Fig. 4 Cylinder surface numbering.

$$F_{31} = \frac{A_1}{A_3}F_{13} = \frac{5.543 \times 10^{-05}}{0.5 \times 2.639 \times 10^{-04}}F_{13} = 0.1821 \tag{26}$$

The view factor of surface 3 to itself and the opposite surface 4 is known, using the enclosure Eq. (7): $(F_{33} + F_{34}) = 1 - F_{31} - F_{32}$.

To be able to split F_{33} and F_{34}, the cylindrical ratio for infinite cylinders from Hahne and Bassiouni [8] is used:

$$F_{34} = \frac{1}{\pi^2}\left\{4R\,\ell n(2R) + \frac{1-4R^2}{2R}\,\ell n(4R^2+1) + 4\tan^{-1}\left(\frac{1}{2R}\right)\right\} \quad \left(F_{34} = \frac{2}{\pi} \text{ within } 3.4\% \text{ when } R \le 0.01\right) \tag{27}$$

with $R = r_{\text{eq}}/d_c$. This results in the following view factors:

$$F_{34} = \frac{2}{\pi}(1 - F_{31} - F_{32}) = 0.4047$$

$$F_{33} = \left(1 - \frac{2}{\pi}\right)(1 - F_{31} - F_{32}) = 0.2310$$

Comparing these results with those determined by Feingold [7] (linearly interpolated), results in $F_{34} = 0.437$. This approximation proves to be accurate to within 8%, which is considered to be acceptable for in-plane radiation purposes. A more accurate relation for the view factor between two half cylinders is preferred, but the use of the finite relation of Hahne and Bassiouni [8] compared to Feingold [7] produced a higher inaccuracy. Therefore, the Feingold [7] relation is used.

Using Eq. (9), the Gebhart radiative exchange factors can be determined (assuming an emissivity factor of 0.80 for the PM1000 face sheets and 0.55 for the PM2000 honeycomb). This results in the following view factor and Gebhart factor matrices, given in Tables 4 and 5, respectively.

The effective conduction caused by radiative exchange can now be calculated.

$$k_{34,\text{rad}} = \varepsilon_3 \frac{A_3}{A_{\text{cross}_{\text{section}}}} B_{34} \cdot 4\sigma T_{\text{avg}}^3 L_{\text{eff}} \tag{28}$$

The effective cross-sectional area $A_{\text{cross}_{\text{section}}}$ and effective length L_{eff} of one equivalent cell size are presented in the previous sections for each in-plane direction (Sec. II.C.1 for the L direction and Sec. II.C.2 for the W direction). The effective conductivity caused by radiation in the L direction becomes

$$\begin{aligned} k_{L,\text{rad}} &= \varepsilon_3 \frac{A_3}{A_L} B_{34} \cdot 4\sigma T_{\text{avg}}^3 L_L \\ &= \varepsilon_3 \frac{3 \cdot S_{\text{hex}} \cdot d_c}{S_c d_c} B_{34} \cdot 4\sigma T_{\text{avg}}^3 \cdot \frac{3}{2} \cdot S_{\text{hex}} \\ &= \frac{4.5 \cdot S_{\text{hex}}^2}{S_c} \varepsilon_3 B_{34} \cdot 4\sigma T_{\text{avg}}^3 \end{aligned} \tag{29}$$

The effective conductivity caused by radiation in the W direction becomes

$$k_{W,\text{rad}} = \varepsilon_3 \frac{A_3}{A_W} B_{34} \times 4\sigma T_{\text{avg}}^3 L_W = \varepsilon_3 \frac{3 \times S_{\text{hex}} \times d_c}{1.5 \times S_{\text{hex}} \times d_c} B_{34} \times 4\sigma T_{\text{avg}}^3 S_c = 2S_c \varepsilon_3 B_{34} \times 4\sigma T_{\text{avg}}^3 \tag{30}$$

The total effective conductance through the honeycomb core in the in-plane direction can be written as follows:

Table 4 View factor of four-surface cylinder

$i\backslash j$	1	2	3	4
1	0.00000	0.13271	0.67677	0.19052
2	0.13271	0.00000	0.19052	0.67677
3	0.27071	0.07621	0.45858	0.19450
4	0.07621	0.27071	0.19450	0.45858

Table 5 Gebhart factors of four-surface cylinder ($\varepsilon_f = 0.80$, $\varepsilon_c = 0.55$)

$i\backslash j$	1	2	3	4
1	0.1452	0.2208	0.3170	0.3170
2	0.1452	0.3170	0.3170	0.2338
3	0.2338	0.2338	0.2396	0.2928
4	0.2338	0.2338	0.2928	0.2396

For the L direction

$$k_{L,\text{eff}} = k_{c,\text{eff},L} + k_{c,L,\text{rad}} = \frac{1.5 k_{\text{cm}} t_c}{S_c} + \frac{4.5 \times S_{\text{hex}}^2}{S_c} \varepsilon_3 B_{34} \times 4\sigma T_{\text{avg}}^3 \tag{31}$$

For the W direction

$$k_{W,\text{eff}} = k_{c,\text{eff},W} + k_{c,W,\text{rad}} = \frac{1}{3} \cdot \frac{k_{\text{cm}} t_c S_c}{S_{\text{hex}}^2} + 2 S_c \varepsilon_3 B_{34} \cdot 4\sigma T_{\text{avg}}^3 \tag{32}$$

III. Equivalent Continuum Mechanical Properties for Honeycomb Core

The effective mechanical properties of the honeycomb-core sandwich panel are calculated in two steps. The first step consists of predicting the effective properties of the honeycomb core in terms of its geometric and material characteristics by means of mechanics of materials approach (see Chapter 4 of Gibson and Ashby [9] for more details). The effective elastic properties determined in the first step are used in conjunction with the classical laminate theory to determine the overall structural behavior of the entire sandwich structure. This approach is common practice and has already been implemented in commercial programs (e.g., HyperSizer™ [3]) for calculating the smeared mechanical properties for stiffened structures, including honeycomb.

IV. Finite Element Models

This section describes the heat transfer and thermomechanical analyses of the honeycomb-core sandwich panel and its simplified (equivalent) shell structure. The thermostructural analyses were performed using the FE analysis code Abaqus® [10].

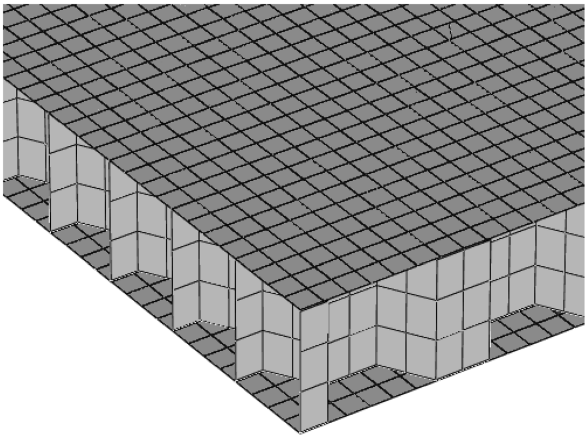

Fig. 5 Finite element mesh of honeycomb sandwich panel.

A. Detailed Finite Element Model of Sandwich Panel

In the FE model of the honeycomb-core sandwich panel, two face sheets and the honeycomb core are modeled by shell elements in full detail, as shown in Fig. 5. Two different FE models having the same mesh are created: a thermal FE model and a structural FE model. The honeycomb core is tied from top and bottom to the top and bottom face sheets, respectively. Consequently, the honeycomb core and face sheets share the same degrees of freedom at their interfaces (i.e., the same temperature in the thermal FE model and the same translations and rotations in the structural FE model). The thermomechanical analysis of the sandwich panel is performed as a sequentially coupled thermal-stress analysis, where the temperature field does not depend on the stress field. The temperature field is first calculated in an uncoupled transient heat transfer FE analysis. The temperatures are then read into the stress analysis as a predefined field; the temperature varies with position and is time dependent. The face sheets and honeycomb core are made from 0.25-mm-thick PM1000 and 0.125-mm-thick PM2000, respectively. The thermal and mechanical properties of PM1000 and PM2000 are temperature dependent. The thermal and structural FE models are described in the following paragraphs.

1. *Thermal Finite Element Model*

A four-node heat transfer quadrilateral shell element, having nodal temperature as degrees of freedom, is used to model the honeycomb cell walls and face sheets. The outer face sheet of the sandwich panel is subjected to a transient heat flux (see Fig. 6) which represents the predicted heat loads at a windward location on the IXV (intermediate experimental vehicle), a European Space Agency experimental lifting body reentry vehicle. The initial temperature of the entire sandwich panel is assumed to be 273.15 K before the atmospheric reentry. The thermal boundary condition is characterized by the radiation of the outer face sheet to an ambient sink temperature of 273.15 K with an emissivity factor of 0.8. In addition, the radiative heat exchange between the face sheets and honeycomb cell walls is included in the thermal FE model. An adiabatic boundary condition is assumed at the back surface of the interior face sheet, which is in contact with the insulation in a TPS design.

The gap radiation used in the transient thermal FE analysis is corrected to incorporate all multiple reflections (i.e., for the face sheets) using Eq. (33). The same relation is used for the interaction between the face sheets and the honeycomb walls, as well as in between the honeycomb walls:

$$\left.\begin{aligned} &\text{Abaqus gap radiation relation: } q_{12,\text{rad}} = \frac{A_1 F \sigma (T_1^4 - T_2^4)}{\frac{1}{\varepsilon_1} + \frac{1}{\varepsilon_2} - 1} \\ &\text{Gebhart radiative heat exchange: } q_{12,\text{rad}} = \varepsilon_1 A_1 B_{12} \sigma (T_1^4 - T_2^4) \end{aligned}\right\}$$
$$\Rightarrow F = \varepsilon_1 B_{12} \left(\frac{1}{\varepsilon_1} + \frac{1}{\varepsilon_2} - 1 \right) \tag{33}$$

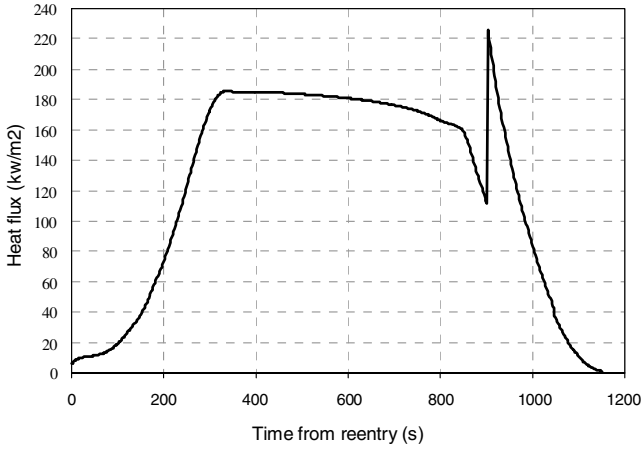

Fig. 6 Representative aerodynamic heat flux profile for the IXV reentry vehicle.

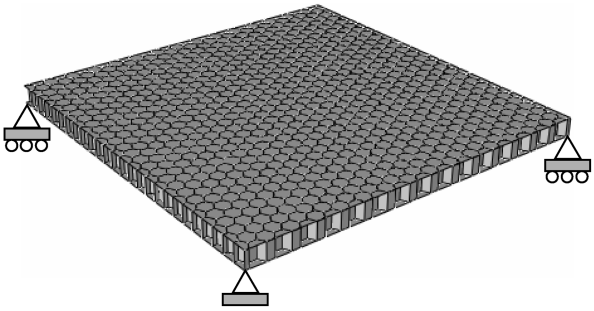

Fig. 7 Mechanical boundary conditions.

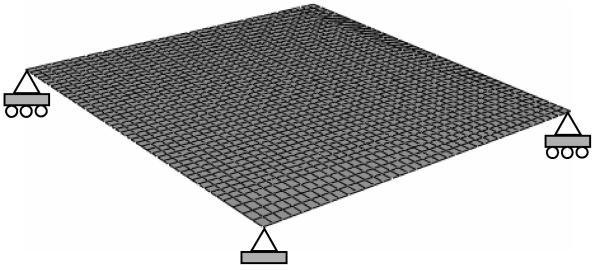

Fig. 8 Finite element mesh and mechanical boundary conditions of the equivalent shell structure.

2. Structural Finite Element Model

A 3-D structural FE model is developed to predict the mechanical response of the sandwich panel to the applied temperature field (as results of transient heat transfer analysis). A four-node, linear, reduced integration, quadrilateral shell element is used to model the honeycomb core (honeycomb cell walls) and face sheets. This element is robust and suitable for a wide range of applications. No mechanical loads are applied to the structural FE model. The external loads include the temperature field of the face sheets and honeycomb. The sandwich panel is allowed to freely expand due to the thermal loads.

Figure 7 shows the application of mechanical boundary conditions. All six rigid body motions are removed from the model by applying necessary constraints at the four corners of the panel. A free–free boundary condition is assumed for the extraction of the natural frequencies and corresponding modes.

B. Finite Element Model of the Equivalent Laminate Shell

Thermal and structural FE models of the equivalent shell structure were constructed. The effective thermal properties of the honeycomb core were determined using both the Swann–Pittman and alternative methods. Using classical laminate theory, a laminate structure (continuum shell composite layup), which is composed of two face sheets and one continuum honeycomb core, was constructed. Abaqus models a continuum shell composite layup using continuum shell elements that fully discretize each ply but have a kinematic behavior that is based on shell theory. Continuum shell composite layups are expected to have a single element through their thickness, and that single element contains multiple plies that are defined in the ply table. The thermal and structural element types are similar to those of the honeycomb-core sandwich panel (previous paragraph). Figure 8 shows the FE mesh and mechanical boundary conditions of the equivalent shell structure. The front face of the equivalent shell is subjected to the transient heat flux of the IXV vehicle (see Fig. 6). Consistent with the thermal FE model, the initial temperature of the panel is assumed to be 273.15 K before the atmospheric reentry. The thermal boundary condition is characterized by radiation to an ambient sink temperature of 273.15 K from the outer surface of the shell with an emissivity factor of 0.8. An adiabatic boundary condition is assumed for the cold back face.

V. Numerical Results

This section describes the heat transfer FE analysis results, eigenvalues and corresponding modes, and thermomechanical FE analysis results of the detailed honeycomb-core sandwich panel and its equivalent shell structure.

A. Input Parameters

The thermal properties of the face sheet (PM1000) and honeycomb-core (PM2000) material are listed in Table 6. These

Table 6 Material properties of the sandwich structure

Material	Temp., °C	Temp., K	ρ, kg/m^3	C_p, J/kg K	k, W/m K	E, 10^9 Pa	α, 10^{-6}/K	ε
PM1000	20	293	8240	440	12.0	185	12.9	0.80
	100	373	8240	471	14.0	180	13.2	0.80
	300	573	8240	547	19.1	169	14.1	0.80
	700	973	8240	699	29.3	145	15.8	0.80
	1100	1373	8240	852	39.5	109	17.5	0.80
PM2000	20	293	7180	480	6.3	218	10.4	0.55
	100	373	7161	502	7.6	211	11.2	0.55
	300	573	7109	557	9.7	194	12.4	0.55
	700	973	6987	668	12.9	157	13.8	0.55
	1100	1373	6830	779	15.6	119	15.9	0.55

Table 7 Resulting effective conductivities in T direction for (ε_{cm}, $\varepsilon_f = 0.80$, and $\varepsilon_c = 0.55$)

		Swann–Pittman method			Alternative method				
Temp., °C	Temp., K	k_{cm}, W/m K	$k_{c,rad}$, W/m K	$\boldsymbol{k_{total}}$, **W/m K**	k_{cm}, W/m K	$k_{c,rad,dir}$, W/m K	$k_{c,rad,indir}$ [W/m K]	$k_{c,rad}$, W/m K	$\boldsymbol{k_{total}}$, **W/m K**
0	273	0.185	0.019	**0.204**	0.185	0.007	0.013	0.020	**0.205**
20	293	0.197	0.023	**0.221**	0.197	0.009	0.016	0.025	**0.223**
100	373	0.238	0.048	**0.286**	0.238	0.018	0.034	0.052	**0.290**
300	573	0.303	0.176	**0.478**	0.303	0.066	0.122	0.188	**0.491**
700	973	0.402	0.860	**1.261**	0.402	0.324	0.598	0.922	**1.324**
1100	1373	0.487	2.415	**2.902**	0.487	0.911	1.681	2.591	**3.078**
1350	1623	0.551	3.988	**4.539**	0.551	1.504	2.776	4.280	**4.831**

Table 8 Resulting alternative method effective conductivities in L/W directions ($\varepsilon_f = 0.80$ and $\varepsilon_c = 0.55$)

		L direction			*W* direction		
Temp., °C	Temp., K	k_{cm}, W/m K	$k_{c,rad}$, W/m K	$\boldsymbol{k_{total}}$, **W/m K]**	k_{cm}, W/m K	$k_{c,rad}$, W/m K	$\boldsymbol{k_{total}}$, **W/m K]**
0	273	0.139	0.010	**0.149**	0.092	0.013	**0.106**
20	293	0.148	0.012	**0.160**	0.099	0.016	**0.115**
100	373	0.178	0.025	**0.204**	0.119	0.034	**0.153**
300	573	0.227	0.092	**0.319**	0.151	0.122	**0.274**
700	973	0.301	0.449	**0.751**	0.201	0.599	**0.800**
1100	1373	0.365	1.262	**1.627**	0.243	1.683	**1.926**
1350	1623	0.413	2.084	**2.498**	0.276	2.779	**3.055**

materials can carry thermal loads up to 1300°C. For the equivalent shell model, the PM2000 core material properties are transformed into effective thermal and mechanical properties, which are listed in Tables 7 and 8.

Results for the effective conductivity coefficients of the Swann–Pittman method and the new alternative method as a function of the temperature (constant emissivity used for this example) are given in Table 7. The in-plane effective conductivities for the alternative method are presented in Table 8. The results show that the radiative part of the effective conductivity of the alternative method is slightly higher. The effect of these differences is presented in the next section. To investigate the accuracy of both methods for other parameters, many case studies have to be compared, by varying the configuration parameters, emissivities, and environmental cases. These case studies are, however, not included in this paper.

B. Thermal Responses

To check the response of both equivalent methods for the numerical example, a constant flux case is applied (70 kW/m^2) and compared with the results of a detailed analytical thermal model (10 nodes through the core thickness). The results, presented in Fig. 9, show that the alternative method shows practically the same results as the generally accepted Swann–Pittman method, which is a

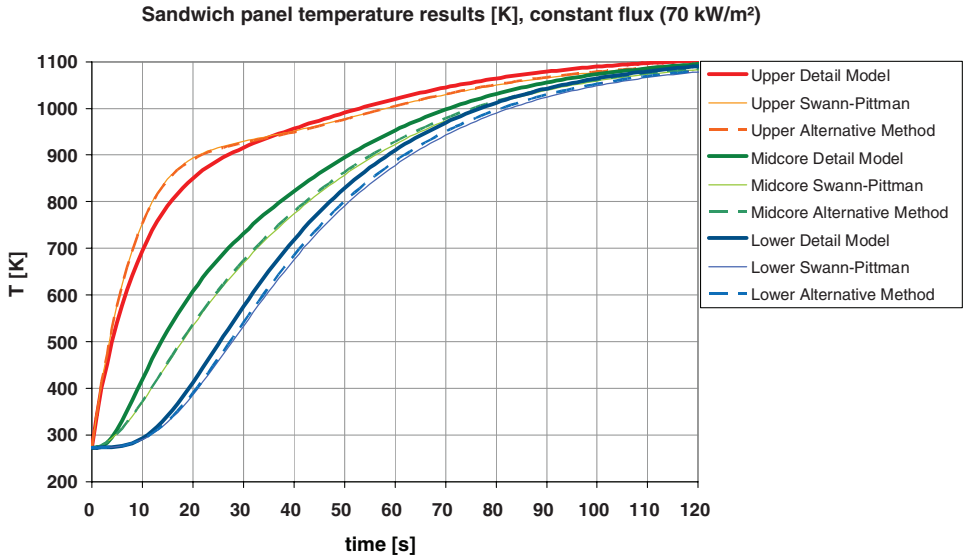

Fig. 9 Constant warm-up (70 kW/m^2) comparison.

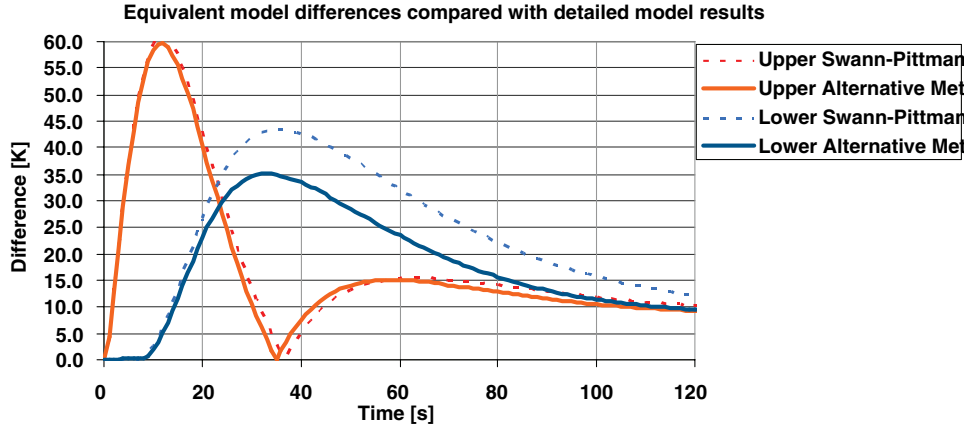

Fig. 10 Constant flux warm-up accuracy.

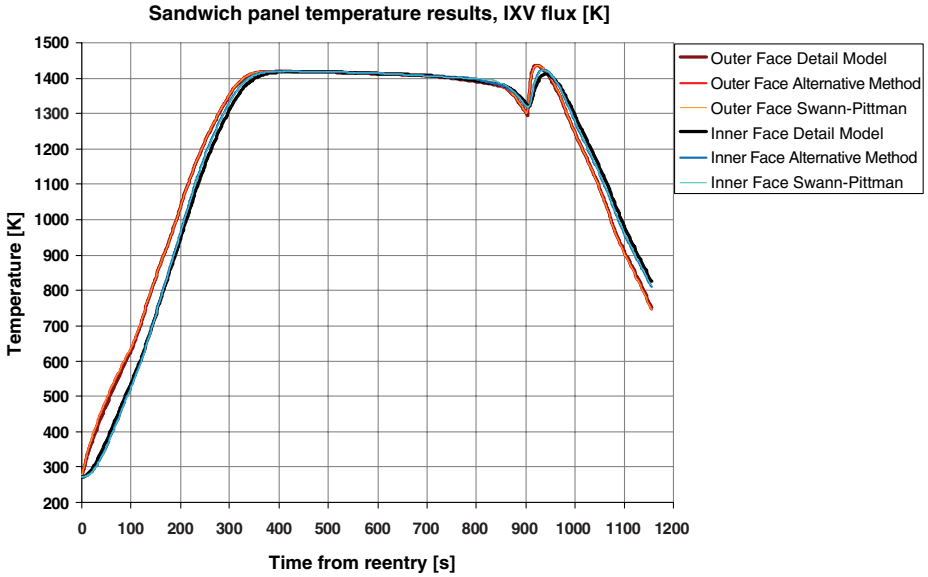

Fig. 11 Time history of the temperatures at outer and inner face sheets and midsurface of the honeycomb core for the detailed model sandwich panel and the equivalent laminate structures.

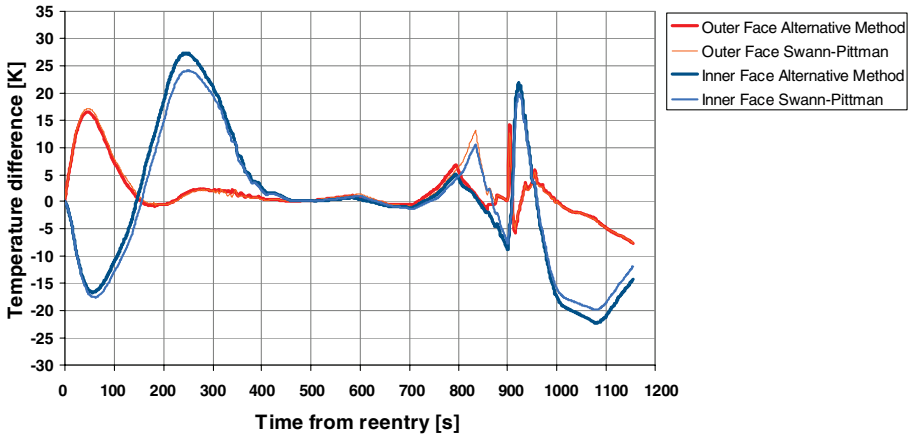

Fig. 12 Equivalent model temperature accuracy (IXV flux).

good first validation of the alternative method. It can also be observed that both equivalent models show a steeper warm up at the start. This is partly caused by neglecting the higher-order terms in Eqs. (4) and (13) and partly by the thermal inertia of the core, causing a nonlinear temperature gradient over the honeycomb, whereas the methods assume a developed close-to-linear gradient over the core material. These effects are inherent in the modeling of the radiation as a material property of the honeycomb core (which has no knowledge of the face sheet temperatures), including the radiative exchange in the thermal inertia of the conductive path. This inaccuracy can only be avoided by including the face sheet temperatures in a subroutine. This would increase the transient accuracy, but also the modeling and analysis time and model complexity. For the purpose of large-scale FE models of sandwich structure this is a major drawback and, therefore, the transient inaccuracy of the equivalent shell method can be considered a limitation, which can be taken into account in an error budget.

A more detailed graph of the temperature error of the methods is presented in Fig. 10. The results show that both equivalent models become much more accurate when the transient effect becomes less dominant and the internal gradient has had time to develop. The accuracy of the temperature results increases from 60 K during the steep warm up, to within 10 K near steady-state results. This clearly shows the limitation in accuracy of the equivalent shell methods for steep transient fluctuations of the heat loads.

Comparisons between the temperature histories obtained by using the continuum core model (for both the Swann–Pittman and alternative methods) and those obtained from the detailed FE model of the sandwich panel for the reentry flux profile (IXV reentry vehicle) presented in the previous paragraph are shown in Fig. 11. This figure shows the time history of the temperatures at the center of the outer and inner face sheets, and the midsurface of the honeycomb core for the three models. A good general correlation between the temperatures predicted by the equivalent laminate structures and those of the sandwich panel in the face sheets and midsurface can be observed in Fig. 11.

Table 9 Eigenfrequencies of sandwich panel and equivalent shell structure

Eigenmode	Eigenfrequency, Hz		Error, %
	Sandwich panel	Equivalent shell	
1	946	959	1.4
2	1441	1436	−0.3
3	1791	1769	−1.2
4	2367	2422	2.3
5	2370	2423	2.2

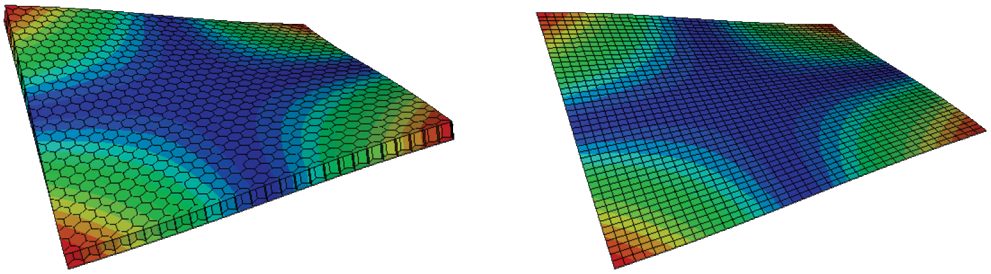

Fig. 13 First eigenmode for the sandwich panel (left) and equivalent shell structure (right).

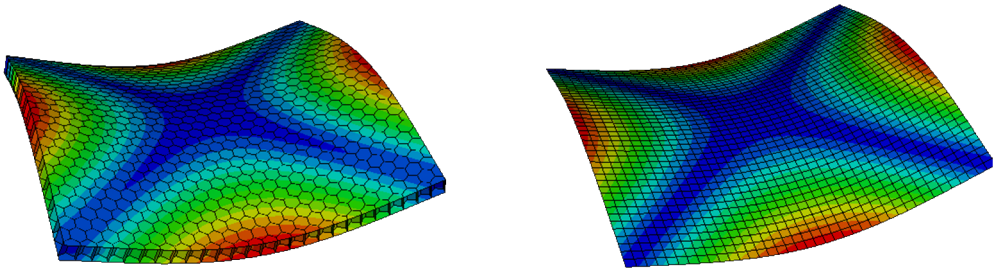

Fig. 14 Second eigenmode for the sandwich panel (left) and equivalent shell structure (right).

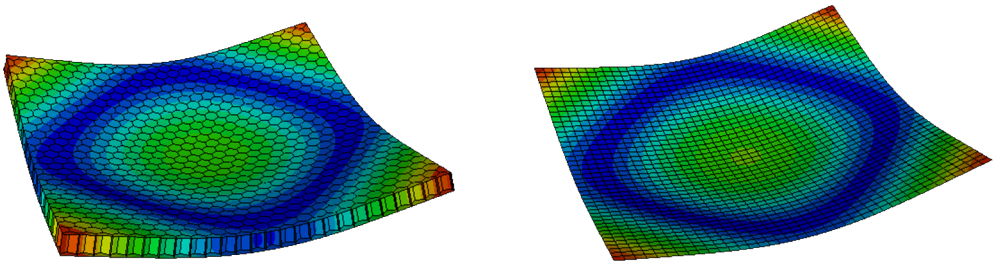

Fig. 15 Third eigenmode for the sandwich panel (left) and equivalent shell structure (right).

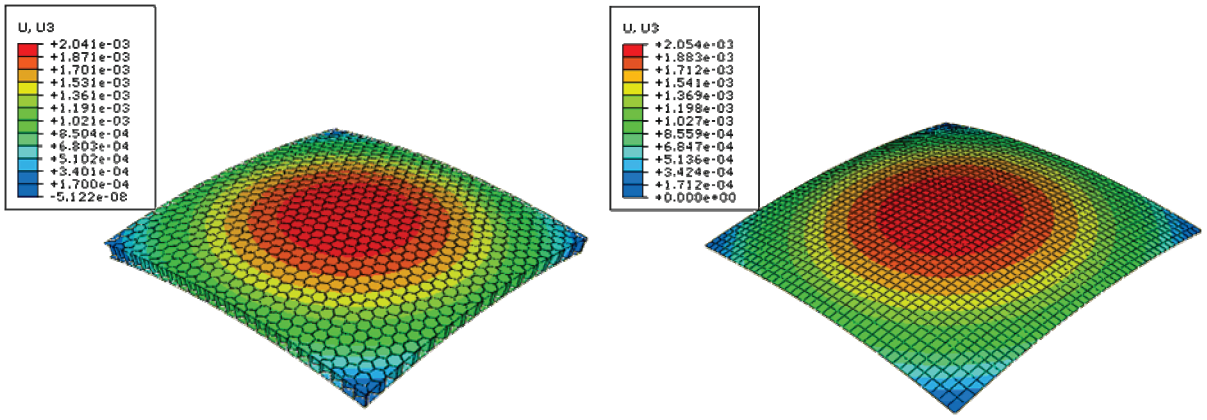

Fig. 16 Deformed shape of sandwich panel (left) and equivalent shell structure (right) under heating on top.

The differences between the temperatures of the detailed honeycomb-core sandwich and the equivalent shell models are presented in Fig. 12. The results show that the temperatures of the equivalent models are accurate to within 30 K (less than 5% of the absolute temperature) during the transient phases (steep warm up or cool down) and within 5 K for the stationary condition (less than 1% of absolute temperature between 400 and 800 s of reentry phase).

C. Free Vibration Eigenfrequencies

Comparisons between free vibration frequencies obtained by using the continuum core model (equivalent laminate shell structure) and the detailed FE model are presented in this section. The first 20 free vibration eigenfrequencies and corresponding eigenmodes of both the sandwich panel and the equivalent shell structure are

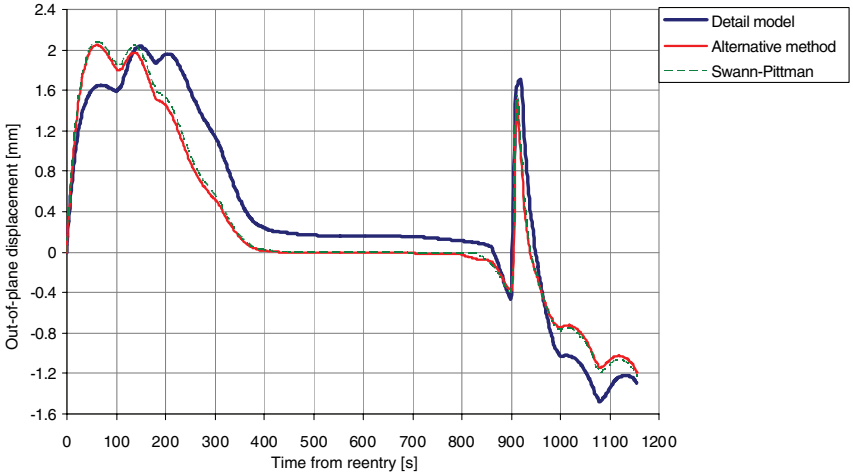

Fig. 17 Time history of the out-of-plane displacement of sandwich panel and equivalent shell structure.

extracted. The first six eigenfrequencies which correspond to the six rigid body modes are near zero for both structures. The first five (nonzero) eigenfrequencies of both structures are reported in Table 9. The reported eigenfrequencies show that the equivalent laminate shell structure accurately predicts the eigenfrequencies of the original honeycomb sandwich panel. The error of eigenfrequency prediction of the first five nonzero eigenfrequencies is less than 2.5%.

The eigenmodes of the sandwich panel and equivalent shell structure corresponding to the first three nonzero eigenvalues are presented in Figs. 13–15. The deformed shapes for the given eigenmodes are the same.

D. Thermomechanical Responses

The thermal deformations of the sandwich panel (detailed model) and its corresponding equivalent shell structure induced by transient heating are discussed in this section.

Figure 16 shows the deformed shapes of the sandwich panel and equivalent shell structure subjected to the transient heat flux at the outer surface of the outer face sheet. The deformed shape of both models is similar. The history of maximum out-of-plane displacements of the sandwich panel and equivalent laminate structure are shown in Fig. 17. In general, there is a good agreement of thermomechanical behavior between the sandwich panel and the equivalent laminate structure. The difference between the maximum out-of-plane displacements of the detailed sandwich model and equivalent laminate model is less than 2%.

The out-of-plane displacement histories of a point in the middle of the face sheet for the sandwich panel and equivalent laminate structure are shown in Fig. 17. The maximum out-of-plane displacement of the sandwich panel occurs later than the one for the equivalent laminate shell structure. This can be explained by the inertia in the development of a linear gradient in the honeycomb-core elements, on which the accuracy of the equivalent models is largely dependent. Aside from the time shift caused by this effect, the out-of-plane displacements of the equivalent models are similar to those of the detailed model. The difference between the peak displacements (equivalent model compared to detailed model) is less than 2%.

E. Problem Size and Computational Time

The FE model size and computational time of thermal and thermomechanical analyses of the sandwich panel and corresponding equivalent shell model are compared in this section. Table 10 depicts the number of elements and nodes, total number of variables in the model (degrees of freedom plus any Lagrange multiplier variables), and total CPU time of thermal and thermomechanical FE analyses for both the sandwich panel and the corresponding equivalent shell structure. The right column of this table shows the reduction factor for the problem size and computational time. The computational time for the thermal and thermomechanical FE analyses is dramatically reduced by replacing the detailed sandwich panel FE model with its equivalent laminate structure FE model (the computational time reduction is more than 12 times for thermal analysis and more than 71 times for thermomechanical analysis of the given example). It should be noted that the computational time for the structural FE analysis of both structures includes the time for the extraction of the eigenfrequencies, as well as 1155 s of aerodynamic heating of the outer face sheet.

VI. Conclusions

Application of equivalent thermal and mechanical properties of honeycomb core into a laminate shell structure results in reasonably accurate thermomechanical behavior and at the same time decreases the computational costs of the FE analyses considerably. For the presented example, the CPU time is reduced by factors of 13 and 72, respectively, for the thermal and structural analysis.

The new alternative method allows for different materials for each face sheet and the honeycomb core through the incorporation of different emissivities and honeycomb-core in-plane equivalent conductivity properties. The proposed method is attractive for the FE modeling of an entire reentry vehicle TPS where sandwich panels

Table 10 Comparison of problem size and CPU time between honeycomb-core sandwich panel and equivalent laminate shell structure (workstation specifications: Xeon® Processor 3.00 GHz, 3 GB RAM)

Model and analysis type	Problem size and computational time	Honeycomb-core sandwich panel	Equivalent shell structure	Reduction factor
Thermal analysis	No. of elements	35,880	1755	20.4
	No. of nodes	38,084	1840	20.7
	CPU, s	**4566**	**362**	**12.6**
Thermal-stress analysis	No. of elements	35,880	1755	20.4
	No. of nodes	38,084	1840	20.7
	CPU, s	**21,996**	**307**	**71.6**

(made of different materials) are used as load-carrying structures. The analysis method can therefore be beneficial for the conceptual design of reentry vehicle TPS where time and computational resources are generally limited.

Acknowledgments

The authors would like to acknowledge the Netherlands Agency for Aerospace Programs for their support to the hot structures program. We would also like to thank Dutch Space and Netherlands Organization for Applied Scientific Research for giving us the opportunity to publish this paper. The European Space Agency and Next Generation Launcher Prime are acknowledged for providing the heat flux profile of the IXV reentry vehicle.

References

[1] Fatemi, J., Birjmohan, S., Rijkeboer, M., and Bakker, M. C. M., "Analysis and Testing of a Metallic Thermal Protection System for RLV Application," *Proceedings of the 4th International Symposium Atmospheric Reentry Vehicles & Systems*, Assoc. Aeronautique et Astronautique de France, Paris, France, March 2005, pp. 1–10.

[2] Swann, R. T., and Pittman, C. M., "Analysis of Effective Thermal Conductivities of Honeycomb-Core and Corrugated-Core Sandwich Panels," NASA TN D-714, April 1961.

[3] Collier, C., Yarrington, P., Pickenheim, M., and Bednarcyk, B., "An Approach to Preliminary Design and Analysis," AIAA Paper 2007-2176, April 2007.

[4] Blosser, M. L., "Advanced Metallic Thermal Protection Systems for Reusable Launch Vehicles," Ph.D. Dissertation, Mechanical and Aerospace Engineering Dept., Univ. of Virginia, Charlottesville, VA, 2000.

[5] Gebhart, B., *Heat Transfer*, McGraw–Hill, New York, 1971.

[6] Sparrow, E. M., and Cess, R. D., *Radiation Heat Transfer*, Brooks/Cole Publishing, Belmont, CA, 1970.

[7] Feingold, A., "Radiant-Interchange Configuration Factors Between Various Selected Plane Surfaces," *Proceedings of the Royal Society of London A*, Vol. 292, No. 1428, 1966, pp. 51–60. doi:10.1098/rspa.1966.0118

[8] Hahne, E., and Bassiouni, M. K., "The Angle Factor for Radiant Interchange Within a Constant Radius Cylindrical Enclosure," *Letters in Heat and Mass Transfer*, Vol. 7, No. 41980, pp. 303–309. doi:10.1016/0094-4548(80)90015-6

[9] Gibson, L. J., and Ashby, M., *Cellular Solids, Structures and Properties*, 2nd ed., Cambridge Univ. Press, Cambridge, England, U.K., 1997, Chap. 4.

[10] Abaqus® User's Manual, Ver. 6.7, SIMULIA, Dassault Systèmes, 2007.

K. Wurster
Associate Editor